Phosphate Sensing by Fluorescent Reporter Proteins Embedded in Polyacrylamide Nanoparticles

Honghao Sun,[†,*] Anne Marie Scharff-Poulsen,[‡] Hong Gu,[‡,¶] Iver Jakobsen,[‡] Jens M. Kossmann,[§] Wolf B. Frommer,[⊥] and Kristoffer Almdal[†]

[†]Polymer and [‡]Biosystems Departments, Risø, Technical University of Denmark, Roskilde 4000, Denmark, [§]Institute of Plant Biotechnology, University of Stellenbosch, South Africa, and [⊥]Department of Plant Biology, Carnegie Institution, 260 Panama Street, Stanford, California 94305-4101. [¶]Present address: Faculty of Life Science, University of Copenhagen, Denmark.

ABSTRACT Phosphate sensors were developed by embedding fluorescent reporter proteins (FLIPPi) in polyacrylamide nanoparticles with diameters from 40 to 120 nm. The sensor activity and protein loading efficiency varied according to nanoparticle composition, that is, the total monomer content (% T) and the cross-linker content (% C). Nanoparticles with 28% T and 20% C were considered optimal as a result of relatively high loading efficiency (50.6%) as well as high protein activity (50%). The experimental results prove that the cross-linked polyacrylamide matrix could protect FLIPPi from degradation by soluble proteases to some extent. This nanoparticle embedding method provides a novel promising tool for *in vivo* metabolite studies. It also demonstrates a universal method for embedding different fragile bioactive elements, such as antibodies, genes, enzymes, and other functional proteins, in nanoparticles for, for example, sensing, biological catalysis, and gene delivery.

KEYWORDS: nanosensor · nanoparticle · phosphate · polyacrylamide · protein

Accurate determination of levels of inorganic phosphate (Pi) is an important application in elucidating plant metabolic processes.[1,2] Unfortunately, very few phosphate sensors have been reported that show high selectivity and sensitivity. Selective and reliable sensing of anions is generally difficult to accomplish because anions often display a high energy of hydration, tautomerism, and low surface-charge density, which makes the recognition of anions less effective.[3,4] Owing to the abundant availability in nature, different sensors based on substrate-specific binding proteins have been developed recently through molecular cloning.[5,6] These sensors demonstrate superior selectivity and reliability compared to those made by chemical synthetic methods.[7] Recently, inorganic phosphate sensing proteins (FLIPPi) that comprise a phosphate binding protein (PiBP) fused in between two different fluorescent reporter proteins has been developed in our group[8] (Figure 1A). The fluorescence resonance energy transfer (FRET) efficiency between the two reporter proteins, cyan fluorescent protein (CFP) and yellow fluorescent protein (YFP), changes as a result of the relative conformational movement of the two lobes on PiBP, when the substrate Pi is bound. Quantification of analyte is obtained through analysis of the ratio between YFP and CFP fluorescence emission intensity, which reflects the FRET efficiency, which in turn is a quantitative proxy for Pi concentration.

Recently, we have developed a pH nanosensor in which the fluorescent dyes are covalently bound and embedded in nanometer-sized cross-linked polymer particles.[9] This technique has several advantages over direct loading of fluorescent probes into cells, which is a classical method for monitoring metabolic processes in living cells: (1) the inert and biocompatible polymer matrix protects the intracellular components from any toxicity of the probes, (2) the polymer matrix can prevent sensor proteins from protease attack, interfacial shearing, and solvent denaturation,[10,11] (3) the nanometer size of the sensors minimizes the physical perturbation of the target cells, and (4) the large surface-to-volume ratio of the sensors provides fast response time.[12–14]

On the basis of the advantages of polymer nanosensors, we embedded FLIPPi inside polyacrylamide particles to develop a robust tool for measuring Pi in single living cells without the need for gene transfection and for measuring extracellular Pi levels. Polyacrylamide gel was employed as matrix because of its biocompatibility[14] and sieve-like structure with pores, which have dimensions comparable to those of protein molecules.[15–23] In this study, we report the

*Address correspondence to honghaosuncn@gmail.com.

Received for review August 14, 2007 and accepted December 12, 2007.

Published online January 1, 2008.
10.1021/nn700166x CCC: $40.75

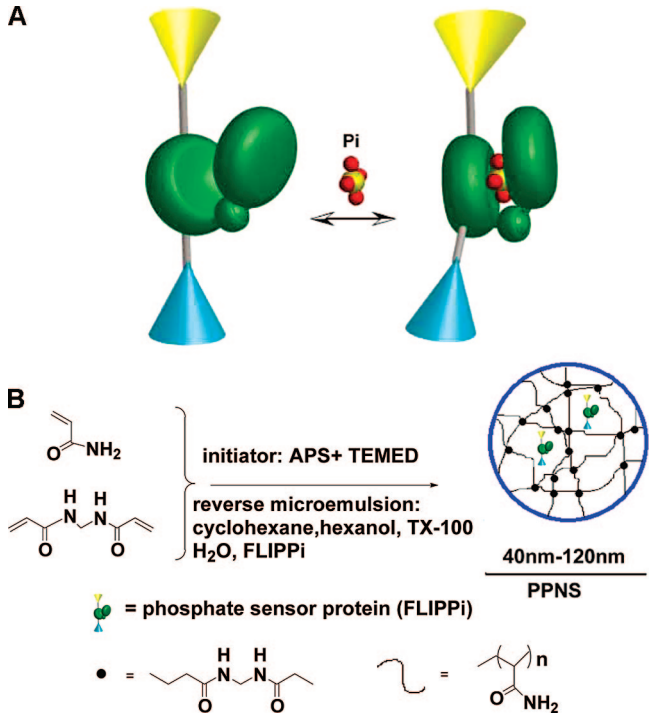

Figure 1. (A) Hypothetical models of the FLIPPi sensor. (B) Synthesis of FLIPPi based on reverse microemulsion polymerization.

relation between activities of the embedded FLIPPi and monomer compositions of polyacrylamide nanoparticles. The size of nanoparticles was studied by scanning electron microscopy (SEM) and dynamic light scattering (DLS). The cross-linked polyacrylamide matrix could protect FLIPPi from degradation by soluble proteases to some extent.

RESULTS AND DISCUSSION

The FLIPPi-embedded nanosensors were initially synthesized following the procedure reported for pH nanosensors.[9] However, the FLIPPi were completely inactivated by the harsh synthesis and purification conditions. We found the following factors had adverse effects on FLIPPi activity: (1) the ionic surfactant dioctyl sulfosuccinate (AOT), (2) the initiators ammonium persulfate (APS) and *N*,*N*,*N*′,*N*′-tetraethylmethylenediamine (TEMED), and (3) the ethanol used for nanoparticle washing. Because of the fragile characteristic of this FLIPPi protein as compared to other proteins and chemical dyes, it was a challenge to achieve polymer inorganic phosphate nanosensors (PPNSs) with active embedded FLIPPi. We explored milder conditions for synthesis and purification to retain the activity of the embedded FLIPPi, and the resulting protocol (Figure 1B) included the use of (1) biocompatible glycol-based surfactant Triton X-100 instead of AOT, (2) minimal amounts of initiators, and (3) extraction and dialysis procedures instead of washing by ethanol during purification. The polymerization was monitored by ^{1}H NMR to ensure that the vinyl group (chemical shift 5.5−6.5 ppm) was consumed completely. To separate the PPNSs from the free FLIPPi, the PPNSs were purified by size exclusion chromatography (SEC) using 3-morpholinopropanesulfonic acid (MOPS) buffer as the mobile phase. The FLIPPi loading efficiency was calculated from the SEC fluorescence detection by computing the signals from the free FLIPPi and PPNSs. The residual content of Triton X-100 in purified PPNSs was measured by HPLC, which indicated that the residual content of Triton X-100 was less than 400 ppm with respect to the particles equivalent to 1.7 μg/mL in 5 mg/mL PPNSs, which is the normal concentration for our routine measurement.

Using the improved synthesis and purification method, we achieved PPNSs with embedded, functional FLIPPi, which respond to Pi titration.

The next experimental step was to improve the degree of embedded protein activity as well as the loading efficiency. From the literature it is known that pore sizes of cross-linked polyacrylamide gels depend in a complex way on two variables: (1) the total monomer content (% T, the sum of acrylamide (AC) and cross-linker methylbisacrylamide (bis-AC) weight ratios in the reaction solution) and (2) the cross-linker content (% C, the weight ratio of bis-AC to total monomer).[24−26] Polyacrylamide gels with different pore sizes have been achieved by combining the variables % T and % C, and gels with different pore sizes are routinely used for size separation of proteins by polyacrylamide gel electrophoresis (PAGE). We hypothesized that the activity and loading efficiency of FLIPPi in polyacrylamide nanoparticles would relate to pore size and thus vary at different monomer compositions. For example, on the one hand bigger pore sizes of nanoparticles could result in increased protein activity because of less conformation change restriction of embedded proteins, but on the other hand, it could cause a lower loading efficiency due to increased leaching of embedded protein. Smaller pore sizes could be expected to have the opposite effect.

Effects of monomer composition on PPNS properties were systematically studied by investigating three total monomer compositions (14%, 28%, and 56% T) in combination with four cross-linking levels (2.0%, 3.8%, 7.4%, and 20.0% C). The monomer compositions of the synthesized nanoparticles, activity of embedded protein, loading efficiency, and particle sizes are reported in Table 1 and Figure 2. Two major trends were observed in several repeated experiments: (1) at constant % C, an increase in % T led to decreased activity of embedded proteins as well as increased loading efficiency, and (2) at constant % T, an increase in % C resulted in higher loading efficiency and lower protein activity. This effect was pronounced, however, only at lower % C (<7.4% C) and seemed to level off or even show the opposite trend at higher % C. Our results demonstrate that the characteristics of the embedded protein are profoundly impacted by monomer composition, and a

TABLE 1. Protein Activity, Particle Size, and Loading Efficiency at Different Monomer Compositions (% T, % C)

%T[a]	% C[b]	protein activity $\Delta R_e/\Delta R_f$ (%)[c]	particle diameter (nm)[d]	loading efficiency (%)[e]
56	20	12	66	68.3
56	7.4	17	55	71.0
56	3.8	21	61	69.5
56	2.0	24	87	64.2
28	20	50	44	50.6
28	7.4	44	42	52.6
28	3.8	53	49	24.1
28	2.0	56	50	23.5
14	20	56	74	18.9
14	7.4	43	95	18.0
14	3.8	67	100	9.1
14	2.0	78	115	9.0

[a]% T = {*m*(AC + bis-AC)/*m*(AC + bis-AC + buffer)}×100. [b]% C = {*m*(bis-AC)/*m*(Ac + bis-AC)}×100. [c]ΔR_e is the YFP/CFP ratio difference of PPNSs between the points saturated with Pi and free of Pi; ΔR_f is the YFP/CFP ratio difference of free FLIPPi between the points saturated with Pi and free of Pi. [d]Hydrodynamic diameter measured by DLS. [e]Calculated from SEC fluorescence spectra.

careful selection of reaction mixture composition will thus allow for tailoring of nanoparticle properties. The choice of optimal monomer composition would depend on the application of the resulting nanoparticles. The combination of a high protein activity and a high loading efficiency was desirable in this study. This disqualified all particles with 14% T because of a very low loading efficiency, and all particles with 56% T were excluded because of a very low protein activity. The remaining particles with 28% T performed moderately well with regard to both protein activity and loading efficiency. The sample with 28% T and 20% C was considered as the optimal PPNS composition as a result of relatively high loading efficiency (50.6%) and high protein activity (50%).

Pore sizes were not measured directly in our experiments, but our results did not disagree with the hypothesis that monomer composition influences pore size, which again influences activity and loading efficiency of embedded protein. The literature reports decreasing pore sizes with increasing % T. Larger pore sizes could lead to more leaching of embedded protein and less restriction of conformation changes, which is well in accordance with our observation of decreased activity of embedded proteins and increased loading efficiency with increasing % T. The cross-linker content % C has been reported to impact the gel structure by a near-parabolic function with minimum pore sizes at about 5% C,[24] which agrees well with our results in the sense that we measured maximum loading efficiency and minimum protein activity at 7.4% C.

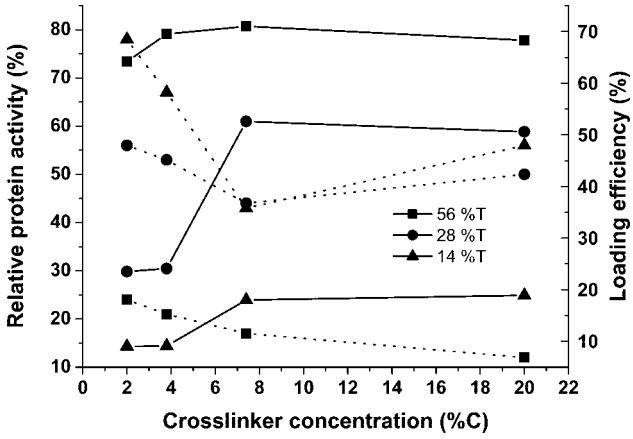

Figure 2. Comparison of relative protein activity (dotted line) and loading efficiency (solid line) at different combinations of total monomers (14%, 28%, 56% T) and cross-linker concentration (2.0%, 3.8%, 7.4%, 20% C), where %T = {*m*(AC + bis-AC)/*m*(AC + bis-AC + buffer)}×100, % C = {*m*(bis-AC)/*m*(Ac + bis-AC)}×100, relative protein activity (%) = $\Delta R_e/\Delta R_f$.

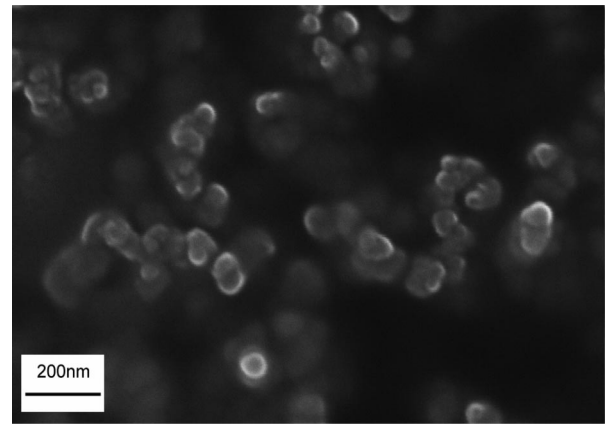

Figure 3. SEM image of gold-coated polyacrylamide PPNS sensors.

PPNSs could be easily dispersed in water by ultrasonic treatment because of the hydrophilic property of the polyacrylamide matrix, and dispersions were stable for weeks. Particle sizes of all dissolved samples were determined by DLS, and their mean hydrodynamic diameters are given in Table 1. The sample with 28% T, 20% C has a mean hydrodynamic diameter of 44 nm in water as determined by DLS, and its SEM result is shown in Figure 3. The particle sizes of PPNSs with 28% and 56% T varied randomly between 42 and 87 nm. These size differences seemed not to relate to monomer composition but might have been caused by minor condition variations in the polymerization process. However, PPNSs with 14% T had larger diameters, possibly because particles with low % T swelled more in water. It was found that after polymerization but before purification of nanoparticles, the PPNSs dispersed in cyclohexane were 2- to 3-fold larger than the initial micelles. It is likely that the increase in diameter was caused by micelle collisions during free radical polymerization, which produces one nanoparticle from multiple micelles.[15,27–29]

The actual loading of PPNSs with FLIPPi was quantified from fluorescence intensity of PPNSs and a standard curve of free FLIPPi. It was found

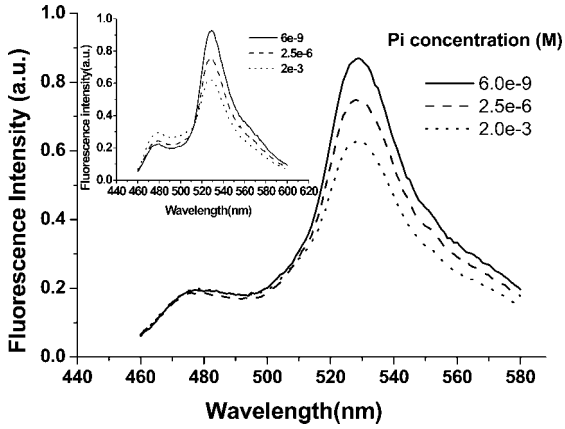

Figure 4. Fluorescence emission spectra of PPNSs (28% T, 20% C) and free FLIPPi (insert) at different phosphate concentrations. PPNSs and FLIPPi were suspended in 20 mM MOPS, pH 7 and excited at 430 nm. For clarity only selected spectra are shown in this figure. Fluorescence intensity is given in arbitrary units.

that for 28% T, 20% C each single PPNS on average contained three FLIPPi molecules. A high dye load per particle is attractive to ensure high sensitivity, and the attempt to load more FLIPPi per particle is in progress.

The PPNS sensors and free FLIPPi were titrated with a phosphate solution. For clarity, only selected fluorescence spectra are shown in Figure 4. The spectra indicate that titration of PPNSs and free FLIPPi with Pi led to small CFP emission increases and large YFP emission decreases, which demonstrates a Pi-dependent decrease in FRET efficiency. Titration curves of 28% T, 20% C PPNSs and free FLIPPi are showed in Figure 5, in which the ratio between the fluorescence emission intensities of YFP (523–533 nm) and CFP (470–480 nm) was plotted against the phosphate concentration of the solution. The PPNSs showed titration curves and FRET properties similar to those of the pure FLIPPi proteins.

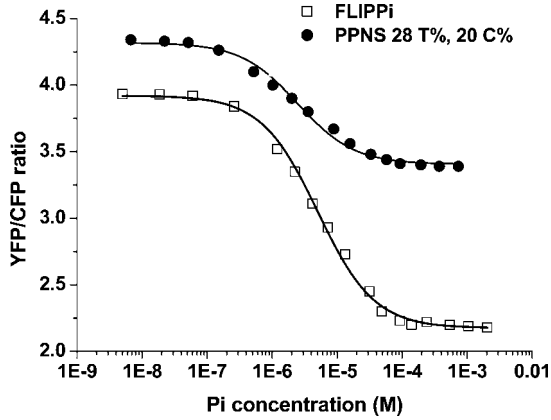

Figure 5. Titration curves of PPNSs (28% T, 20% C) and free FLIPPi. The ratio between the fluorescence emission intensities of YFP (523–533 nm) and CFP (470–480 nm) was plotted against the phosphate concentration of the solution. The data were fit by nonlinear regression to the function describing a single-site binding isotherm: $S = (r - r_{apo})/(r_{sat} - r_{apo}) = [L]/(K_d + [L])$, where S is saturation, [L] is ligand concentration, r is ratio, r_{apo} is ratio in the absence of ligand, and r_{sat} is ratio at saturation with ligand.

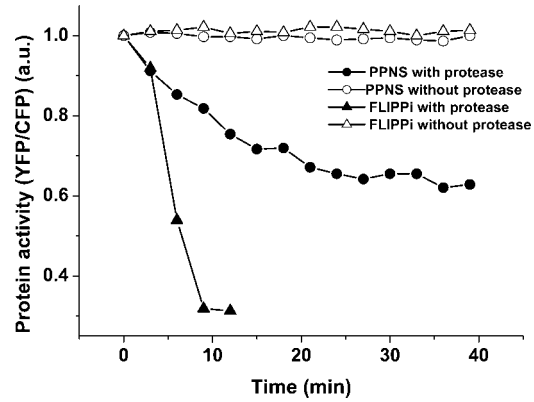

Figure 6. Protease treatment of protein. Reactions were carried out at 25 °C, pH 7 (20 mM MOPS buffer) with an initial protease concentration of 1 μg/mL.

For example, the optimized composition of 28% T, 20% C, which kept 50% activity relative to that of free FLIPPi, displayed a K_d of 2.5 μM, which is close to the FLIPPi K_d of 5 μM. The quantification ranges were also comparable (Figure 5).[8]

It has been reported that a tightly cross-linked polyacrylamide gel can protect immobilized enzymes against digestion by soluble proteases.[11] To evaluate the protease resistance property of PPNSs, the PPNSs and free FLIPPi were challenged with protease (1 μg/mL) and their fluorescence spectra were monitored over time. The FRET efficiency expressed as the CFP/YFP fluorescence ratio of free FLIPPi decreased dramatically, whereas for PPNS samples, the fluorescence spectra showed less change (Figure 6). This proves that the cross-linked polyacrylamide matrix could protect FLIPPi from attack by soluble proteases to some extent. The intensity of YFP, when excited directly at 510 nm, was unchanged (data not shown), which indicates that YFP is not digested by the protease treatment.

The long-term stability of PPNSs is crucial for practical application. We have studied and compared the influence of different purification and storage methods on the stability of PPNSs. PPNSs in MOPS buffer solution stored at 5 or −20 °C lost all activity in 1 week, whereas lyophilized PPNS samples were stable and did not show any decrease of activity in 2 months. Redissolved lyophilized samples had unchanged activity at room temperature for at least 6 h, which would be sufficient for many experiments. The leaching of embedded FLIPPi from purified PPNSs was also investigated by dissolving lyophilized PPNS samples in buffer and subjecting them to SEC. This process was monitored by a fluorescence detector, and no free proteins were detected. This proved that the proteins did not leach out from the polyacrylamide nanoparticles after being embedded.

CONCLUSIONS

We have developed a series of new stable PPNSs made by embedding FLIPPi in a polyacrylamide ma-

trix through water-in-oil inverse microemulsion polymerization and purified by size exclusion chromatography, yielding particles 40–120 nm in diameter. PPNSs have binding properties similar to those of free FLIPPi and display enhanced resistance toward protease digestion compared to the free protein. On the basis of the current results, this nanoparticle embedding method provides a novel promising tool for *in vivo* metabolite studies. It also demonstrates a universal method for embedding different bioactive elements, such as antibodies, genes, enzymes and other functional proteins, in nanoparticles for, for example, sensing, biological catalysis, and gene delivery.

EXPERIMENTAL METHODS

Protein Synthesis. The FLIPPi proteins were expressed in *Escherichia coli* BL21(DE3)Gold (Stratagene, USA) and extracted and purified as previously described.[6,8]

Synthesis of Polymeric Pi Nanosensor (PPNS). The monomer solution contained monomers (acrylamide and methylbisacrylamide) with varying compositions in 10 mM MOPS buffer, pH 7.2. A 0.5-mL portion of this monomer solution was added dropwise to 40 mL of cyclohexane solution that was prepared by mixing of 200 mL of cyclohexane, 9.6 g of TritonX-100, and 7.7 g of *n*-hexanol. The reaction mixture was degassed through three freeze-vacuum-thaw cycles and kept under argon. Then 100 uL of FLIPPi was added to the mixture under argon with stirring. Ten microliters of 5% (w/w) ammonium persulfate solution and 10 μL of 10% TEMED were added to initiate the polymerization. The reaction was stirred at room temperature for 12 h, and subsamples were monitored by ^{1}H NMR to ensure complete polymerization. The cyclohexane was removed by rotary evaporation. and the remaining solution was extracted by MOPS (2 mL × 3) and separated by ultracentrifugation (2000*g*, 30 min). The aqueous part was dialyzed through a dialysis cassette (MWCO 10 kDa, Pierce) immersed in continuously stirred MOPS buffer to remove the surfactant and *n*-hexanol.

Purification and Storage of Nanosensors. In order to separate free proteins from the polymeric nanoparticles, the samples were passed through a SEC column (HiPrepTM 16/60, Amersham Biosciences) at a flow rate of 0.9 mL/min using 0.02 M MOPS buffer, pH 7 as mobile phase. All eluents were monitored by a fluorescence detector (RF-10AXL, Shimadzu) with excitation and emission wavelengths at 488 and 528 nm, respectively. Subsequently, the SEC fractions containing PPNSs were subjected to lyophilization to give a white solid that was stored at −20 °C.

Protease Resistance Experiments. Proteolytic degradation may contribute significantly to activity loss during *in vivo* application of free FLIPPi. In order to evaluate the protease resistance property of PPNSs, the PPNS samples were treated with 1 μg/mL protease (~5.69 U/mg, Fluka) in MOPS buffer at 25 °C, and their fluorescence spectra were monitored over time.

SEM Imaging. A 10-mg sample of PPNSs was dispersed in 1 mL of water and sonicated for several minutes to prevent aggregation of particles. Then a drop of the PPNS solution was placed on a piece of glass microslide. The sample was then sputter coated with gold and visualized using a Zeiss Supra 35 scanning electron microscope.

Dynamic Light Scatting Measurement. A 1.5-mL sample of PPNS solution (5 mg/mL) in milliQ water was sonicated and filtered thorough a 0.45-μM filter. The samples were measured with BI-200SM (Brookhaven Instruments Corporation) DLS instrument.

Fluorescence Spectra. The fluorescence spectra were measured on FL 920 spectrometer (Edinburgh Instruments).

Residual Triton X-100 Analysis. The PPNSs samples were analyzed by HPLC at a flow rate 1.5 mL/min using acetonitrile/water mixture (1/1 by vol) as mobile phase and a CN modified silica column (see Figure 4S, Supporting Information). The eluent was monitored by a UV–vis detector (SPD-M10A, Shimadzu) at 227 nm. Triton X-100 was quantified on the basis of a calibration curve in the concentration range $0.0035 \leq c_{\text{TritonX-100}}$ (mg/mL) ≤ 3.5.

Acknowledgment. This work was supported by the Human Frontier Science Program, Grant RGP0041/2004C.

Supporting Information Available: Comparison of effect of % T/% C on relative protein activity (Figure S1) and loading efficiency (Figure S2), demonstration of PPNS reversibility (Figure S3), and HPLC-UV/vis spectra of pure Triton X-100 and unpurified and purified PPNSs (Figure S4). This material is available free of charge *via* the Internet at http://pubs.acs.org.

REFERENCES AND NOTES

1. Alberts, B.; Bray, D.; Lewis, J.; Raff, M.; Roberts, K.; Watson, J. D. *Molecular Biology of the Cell*, 3rd ed.; Garland Publishing: New York, 1994.
2. Salins, L. L. E.; Deo, S. K.; Daunert, S. Phosphate binding protein as the biorecognition element in a biosensor for phosphate. *Sens. Actuators, B* **2004**, *97*, 81–89.
3. Beer, P. D.; Gale, P. A. Anion recognition and sensing: The state of the art and future perspectives. *Angew. Chem., Int. Ed.* **2001**, *40*, 486–516.
4. Aldakov, D.; Anzanbacher, P., Jr. Sensing of aqueous phosphate by polymers with dual modes of signal transduction. *J. Am. Chem. Soc.* **2004**, *126*, 4752–4753.
5. Okumoto, S.; Looger, L. L.; Micheva, K. D.; Reimer, R. J.; Smith, S. J.; Frommer, W. B. Detection of glutamate release from neurons by genetically encoded surface-displayed FRET nanosensors. *Proc. Natl. Acad. Sci. U.S.A.* **2005**, *102*, 8740–8745.
6. Fehr, M.; Frommer, W. B.; Lalonde, S. Visualization of maltose uptake in living yeast cells by fluorescent nanosensors. *Proc. Natl. Acad. Sci. U.S.A.* **2002**, *99*, 9846–9851.
7. Kuo, L-J.; Liao, J-H.; Chen, C-T.; Huang, C-H.; Chen, C-S.; Fang, J-M. Two-arm ferrocene amide compounds: Synclinal conformations for selective sensing of dihydrogen phosphate ion. *Org. Lett.* **2003**, *5*, 1821–1824.
8. Gu, H.; Lalonde, S. L.; Looger, L.; Okumoto, S.; Scharff-Poulsen, A. M.; Grossman, A. R.; Kossmann, J.; Jakobsen, I.; Frommer, W. B. A novel analytical method for in vivo phosphate tracking. *FEBS Lett.* **2006**, *580*, 5885–5893.
9. Sun, H. H.; Scharff-Poulsen, A. M.; Gu, H.; Almdal, K. Synthesis and characterization of ratiometric, pH sensing nanoparticles with covalently attached fluorescent dyes. *Chem. Mater.* **2006**, *18*, 3381–3384.
10. Yanaguchi, S.; Yoshimura, I.; Kohira, T.; Tamaru, S.; Hamach, I. Cooperation between artifical receptors and supramolecular hydrogels for sensing and discriminating phosphate derivatives. *J. Am. Chem. Soc.* **2005**, *127*, 11835–11841.
11. Pollak, A.; Blumenfeld, H.; Wax, M.; Baughn, R. L.; Whitesides, G. M. Enzyme immobilization by condensation copolymerization into cross-linked polyacrylamide gels. *J. Am. Chem. Soc.* **1980**, *102*, 6324–6336.
12. Buck, S. M.; Xu, H.; Brasuel, M.; Philbert, M. A.; Kopelman, R. Nanoscale probes encapsulated by biologically localized embeddding (PEBBLEs) for ion sensing and imaging in living cells. *Talanta* **2004**, *63*, 41–59.
13. Chen, Y.; Ji, T. H.; Rosenzweig, Z. Synthesis of glyconanospheres containing luminescent CdSe-ZnS quantum dots. *Nano Lett.* **2003**, *3*, 581–584.
14. Clark, H. A.; Hoyer, M.; Philbert, M. A.; Kopelman, R. Optical nanosensors for chemical analysis inside single living cells. 1. Frabrication, characterization, and methods for intracellular delivery of PEBBLE sensors. *Anal. Chem.* **1999**, *71*, 4831–4836.

15. McAllister, K.; Sazani, P.; Adam, M.; Cho, M. J.; Rubinstein, M.; Samulski, R. J.; DeSimone, J. M. Polymeric nanogels produced via inverse microemulsion polymerization as potential gene and antisense delivery agents. *J. Am. Chem. Soc.* **2002**, *124*, 15198–15207.
16. Murthy, N.; Xu, M. C.; Schuck, S.; Kunisawa, J.; Shastri, N.; Frechet, J. M. J. A macromolecular delivery vehicle for protein-based vaccines: Acid-degradable protein-loaded microgels. *Proc. Natl. Acad. Sci. U.S.A.* **2003**, *100*, 4995–5000.
17. Bu, H. Z.; Mikkelsen, S. R.; English, A. M. NAD(P)H sensors based on enzyme entrapment in ferrocene-containing polyacrylamide-based redox gels. *Anal. Chem.* **1998**, *70*, 4320–4325.
18. Delgado, M.; Spanka, C.; Kerwin, L. D.; Jr., P. W.; Janda, K. D. A tunable hydrogel for encapsulation and controlled release of bioactive proteins. *Biomacromolecules* **2002**, *3*, 262–271.
19. Daubresse, C.; Grandfils, Ch.; Jerome, R. Teyssie, Ph. Enzyme Immoblization in Nanoparticles Produed by Inverse Microemulsion Polymerization. *J. Colloid Interface Sci.* **1994**, *168*, 222–229.
20. Daubresse, C.; Grandfils, Ch.; Jerome, R.; Teyssie, Ph. Enzyme immobilization in reactive nanoparticles produced by inverse microemulsion polymerization. *Colloid Polym. Sci.* **1996**, *274*, 482–489.
21. Herr, A. E.; Singh, A. K. Photopolymerized cross-linked polyacrylamide gels for on-chip protein sizing. *Anal. Chem.* **2004**, *76*, 4727–4733.
22. Xu, H.; Aylott, J. W.; Kopelman, R. Fluorescent nano-PEBBLE sensors designed for intracellular glucose imaging. *Analyst* **2002**, *127*, 1471–1477.
23. Rosenzweig, Z.; Kopelman, R. Analytical Properties and Sensor Size Effects of a Micrometer-Sized Optical Fiber Glucose Biosensor. *Anal. Chem.* **1996**, *68*, 1408–1413.
24. Fawcett, J. S.; Morris, C. J. O. R. Molecular-seive chromatography of proteins on granulated polyacrylamide gels. *Sep. Sci.* **1966**, *1*, 9–26.
25. Ruchel, R.; Brager, M. D. Scanning electron microscopic observations of polyacrylamide gels. *Anal. Biochem.* **1975**, *68*, 415–428.
26. Ruchel, R.; Steere, R. L.; Erbe, E. F. Transmission-Electron Microscopic Observations of Freeze-Etched Polyacrylamide Gels. *J. Chromatogr.* **1978**, *166*, 563–575.
27. Carver, M. T.; Hirsch, E.; Wittmann, J. C.; Fitch, R. M.; Candau, F. Percolation and particle nucleation in inverse microemulsion polymerization. *J. Phys. Chem.* **1989**, *93*, 4867–4873.
28. Morgan, J. D.; Lusvardi, K. M.; Kaler, E. W. Kinetics and mechanism of microemulsion polymerization of hexyl methacrylate. *Macromolecules* **1997**, *30*, 1897–1905.
29. Buruaga, A. S. D.; Cal, J. C. D. L.; Asua, J. M. Modeling inverse microemulsion polymerization. *J. Polym. Sci., Part A: Polym. Chem.* **1999**, *37*, 2167–2178.